

# The COSINE-100 Liquid Scintillator Veto System

G. Adhikari<sup>a</sup>, E. Barbosa de Souza<sup>b</sup>, N. Carlin<sup>c</sup>, J. J. Choi<sup>d</sup>, S. Choi<sup>d</sup>, M. Djamal<sup>e</sup>,  
A. C. Ezeribe<sup>f</sup>, L. E. França<sup>c</sup>, C. Ha<sup>g</sup>, I. S. Hahn<sup>h</sup>, E. J. Jeon<sup>i</sup>, J. H. Jo<sup>b</sup>, W. G. Kang<sup>i</sup>,  
M. Kauer<sup>j</sup>, H. Kim<sup>i</sup>, H. J. Kim<sup>k</sup>, K. W. Kim<sup>i</sup>, S. K. Kim<sup>d</sup>, Y. D. Kim<sup>a,i,l</sup>, Y. H. Kim<sup>i,l,m</sup>,  
Y. J. Ko<sup>i</sup>, E. K. Lee<sup>i</sup>, H. S. Lee<sup>i,l</sup>, J. Lee<sup>i</sup>, J. Y. Lee<sup>k</sup>, M. H. Lee<sup>i,l</sup>, S. H. Lee<sup>i,l</sup>,  
D. S. Leonard<sup>i</sup>, B. B. Manzato<sup>c</sup>, R. H. Maruyama<sup>b</sup>, R. J. Neal<sup>n</sup>, S. L. Olsen<sup>i</sup>, B. J. Park<sup>i,l</sup>,  
H. K. Park<sup>o</sup>, H. S. Park<sup>m</sup>, K. S. Park<sup>i</sup>, R. L. C. Pitta<sup>c</sup>, H. Prihtiadi<sup>i</sup>, S. J. Ra<sup>i</sup>, C. Rott<sup>p</sup>,  
K. A. Shin<sup>i</sup>, A. Scarff<sup>n</sup>, N. J. C. Spooner<sup>n</sup>, W. G. Thompson<sup>b</sup>, L. Yang<sup>q</sup>, G. H. Yu<sup>p</sup>

<sup>a</sup>Department of Physics, Sejong University, Seoul 05006, Republic of Korea

<sup>b</sup>Department of Physics and Wright Laboratory, Yale University, New Haven, CT 06520, USA

<sup>c</sup>Physics Institute, University of São Paulo, 05508-090, São Paulo, Brazil

<sup>d</sup>Department of Physics and Astronomy, Seoul National University, Seoul 08826, Republic of Korea

<sup>e</sup>Department of Physics, Bandung Institute of Technology, Bandung 40132, Indonesia

<sup>f</sup>Department of Physics and Astronomy, University of Sheffield, Sheffield S3 7RH, United Kingdom

<sup>g</sup>Department of Physics, Chung-Ang University, Seoul 06973, Republic of Korea

<sup>h</sup>Department of Science Education, Ewha Womans University, Seoul 03760, Republic of Korea

<sup>i</sup>Center for Underground Physics, Institute for Basic Science (IBS), Daejeon 34126, Republic of Korea

<sup>j</sup>Department of Physics and Wisconsin IceCube Particle Astrophysics Center, University of Wisconsin-Madison, Madison, WI 53706, USA

<sup>k</sup>Department of Physics, Kyungpook National University, Daegu 41566, Republic of Korea

<sup>l</sup>IBS School, University of Science and Technology (UST), Daejeon 34113, Republic of Korea

<sup>m</sup>Korea Research Institute of Standards and Science, Daejeon 34113, Republic of Korea

<sup>n</sup>Department of Physics and Astronomy, University of Sheffield, Sheffield S3 7RH, United Kingdom

<sup>o</sup>Department of Accelerator Science, Korea University, Sejong 30019, Republic of Korea

<sup>p</sup>Department of Physics, Sungkyunkwan University, Suwon 16419, Republic of Korea

<sup>q</sup>Department of Physics, University of California San Diego, La Jolla, CA 92093, USA

---

## Abstract

This paper describes the liquid scintillator veto system for the COSINE-100 dark matter experiment and its performance. The COSINE-100 detector consists of 8 NaI(Tl) crystals immersed in 2,200 L of linear alkylbenzene based liquid scintillator. The liquid scintillator tags between 65 and 75% of the internal <sup>40</sup>K background in the 2–6 keV energy region. We also describe the background model for the liquid scintillator, which is primarily used to assess its energy calibration and threshold.

---

## 1. Introduction

Overwhelming cosmological and astronomical observations have provided strong evidence that the most of the matter in the universe is consists of non-relativistic dark matter [1, 2]. The weakly interacting massive particle (WIMP) is one of the theoretically favored candidates to explain this dark matter [3].

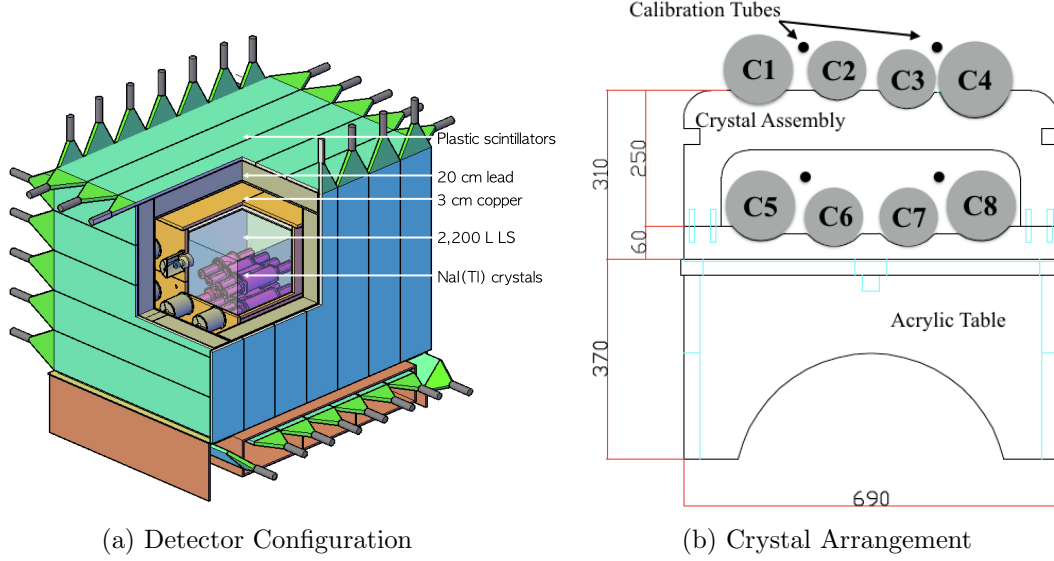


Figure 1: (a) A schematic of the COSINE-100 detector system. 2,200 L of liquid scintillator is filled within an acrylic box inside of a copper box shielding. The top 9 cm of the acrylic box is left unfilled and a nitrogen circulates in this volume. (b) A diagram of the crystal arrangement. An acrylic table supports the crystals. The eight crystals are labeled C1 through C8 and the location of calibration tubes is indicated.

COSINE-100 [4] is a direct dark matter detection experiment to test the DAMA experiment’s detection of an annual modulation signal [5, 6, 7] using the same target material as DAMA. The COSINE-100 detector consists of 8 NaI(Tl) crystals with a total mass of 106 kg, used as active target. The crystals are immersed in 2200 L of liquid scintillator (LS) surrounded by 37 plastic scintillator panels.

It is critical to reduce the background as much as possible for dark matter searches because of the low cross-section of the WIMP-nucleon interaction. The dominant background contributions come from external sources such as decaying radioisotopes in surrounding materials, but remnants of this contribution and the background contribution from materials close to the detector still exist.

The COSINE-100 experiment utilizes the LS and plastic scintillator system as an active veto to reduce the background level by tagging neutrons and  $\gamma$  events from external sources, as well as backgrounds from the internal sources by tagging the escaping  $\gamma$ -rays. The data used in this report were acquired between 20 October 2016 and 19 December 2016, with a total exposure of 59.5 live days. During this period, no substantial environmental abnormalities or unstable detector performance were observed.

## 2. Liquid Scintillator Veto System Configuration

The liquid scintillator in the COSINE-100 detector is contained in an acrylic box. The inner walls of the acrylic container and the outer surfaces of the crystal assemblies are wrapped with Vikuiti-ESR specular reflective films to increase the LS light collection efficiency. The

photons produced in the LS are detected by 18 5-inch R877 photomultiplier tubes (PMTs) from Hamamatsu, attached to the two opposite sides of the box. The minimum distance between the PMTs attached to the crystals and the acrylic box inner wall is approximately 40 cm. Figs. 1a and 1b show a schematic representation of the COSINE-100 detector and shielding structure with the liquid scintillator, and a diagram of the crystal arrangement, respectively. A more detailed description of the detector can be found in [4].

The top 9 cm of the acrylic box holding the LS is left unfilled as a safety margin in the event of a temperature increase that causes an expansion of the LS volume. Gas boil-off from liquid nitrogen is purged into this volume at a rate of 3 liters per minute, to prevent contact with oxygen and water, as well as to maintain a high light yield of the LS. The relative humidity in this space is kept at  $<2.0\%$  and the high heat capacity of the LS helps keep the temperature within the liquid stable at  $24.20 \pm 0.05$  °C.

Signals from the PMTs are collected with two charge-sensitive Analog to Digital Converter (ADC) modules with a sampling rate of 64 MHz [8]. Each ADC module has 32 channels and its peak-to-peak voltage is 2 V with 12-bit resolution. The signals from the 18 PMTs of the LS veto detector are amplified by a factor of 30 before going to the ADC. The LS veto data is taken passively, which means the ADC modules only take data when the NaI(Tl) crystals generate a trigger. Ref. [8] describes details of the trigger algorithm used for the LS veto system.

### 3. Production of Liquid Scintillator

COSINE-100 uses linear alkylbenzene (LAB)-based liquid scintillator [9, 10] which contains 3 g/L of 2,5-diphenyloxazole (PPO) as a primary fluor to convert the captured energy into light and 30 mg/L of 1,4-bis (2- methylstyryl) benzene (bis-MSB) as a wavelength shifter [11]. The emission spectrum of LAB has a maximum at 340 nm, so the wavelength shifter was mixed to the solvent to adjust wavelength of optical photons suitable for the PMTs used in the COSINE-100 experiment. In order to prevent any possible insoluble impurities, LAB is filtered by Meissner filters that have  $0.1 \mu\text{m}$  pore size. After mixing PPO and bis-MSB, the LS is purified using a water extraction method [12] to remove the possible contamination from natural radioisotopes.

Despite the water extraction process for purification, if the LS still has a sufficiently high level of radioisotopes such as  $^{238}\text{U}$  or  $^{232}\text{Th}$ , it will contribute to the background measured in the NaI(Tl) crystals. One needs to carefully measure the background level of the LS so that the background measured in the NaI(Tl) crystals is well understood. For this purpose, a prototype LS detector ( $\sim 70$  mL in volume) read out by 3-inch PMTs was prepared and installed inside the KIMS shielding facility [13] at the Yangyang underground laboratory. A polyethylene shield is good enough to prevent external neutron background events in the alpha band. Alpha events are well separated from gamma events by pulse shape discrimination [14]. The intrinsic  $^{238}\text{U}$  ( $^{232}\text{Th}$ ) chain activity is measured by using the time coincidence between sequential beta- and alpha- (alpha-alpha) decays [15].  $^{238}\text{U}$  and  $^{232}\text{Th}$  activity is measured as 7 ppt and 4 ppt, respectively for the COSINE-100 LS. Therefore, we could

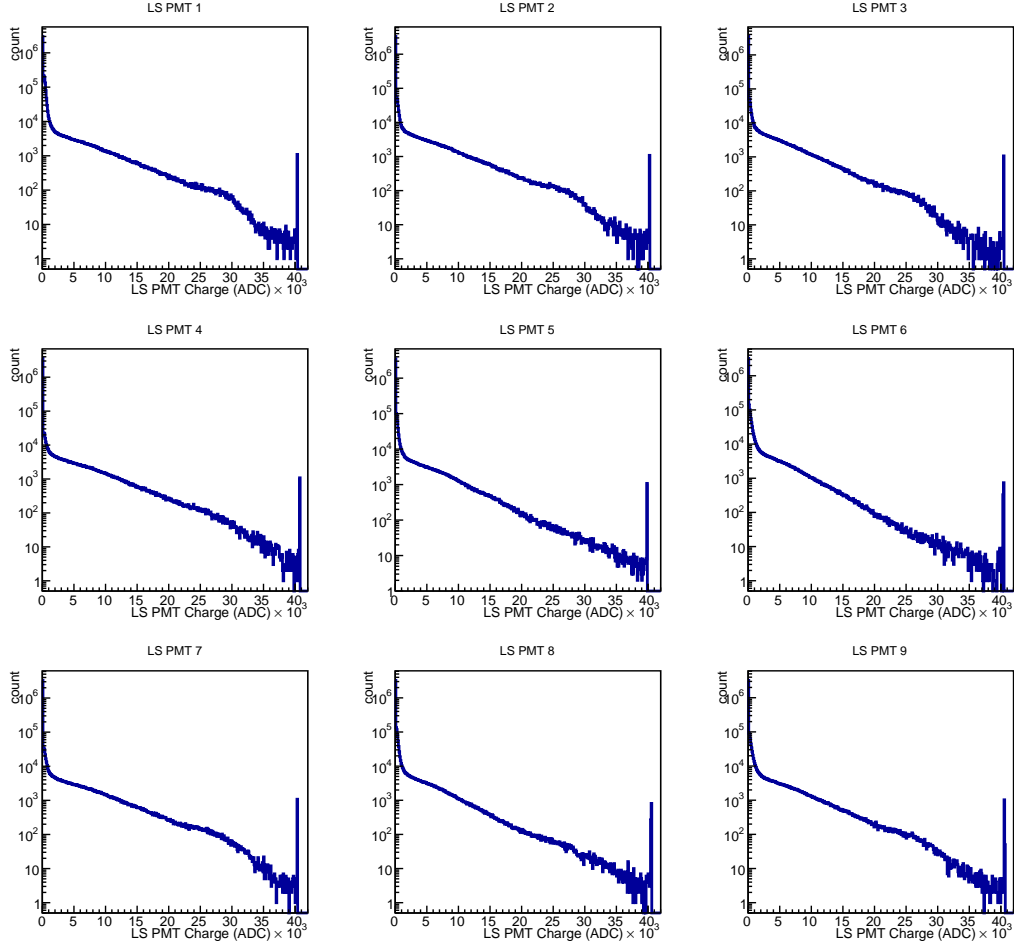


Figure 2: Spectra of nine liquid scintillator PMTs in one side of the COSINE-100 copper shielding, after gain correction, with visible saturation point.

estimate that the background contamination from the LS veto for NaI(Tl) is lower than 0.001 counts/day/keV/kg (dru).

#### 4. Calibration

The 18 PMTs are gain corrected and present very similar energy spectra, as shown in Figure 2. The charges of the 18 PMTs are summed to produce the spectrum of the entire LS veto, and the saturated events are removed to avoid events with misrepresented energies, as seen in Figure 3. The spectrum does not have many features, but it is possible to notice two main shoulders towards the higher energies. These are thought to be coming from energy deposited by gamma rays from  $^{40}\text{K}$  (1.46 MeV) and  $^{208}\text{Tl}$  (2.6 MeV).

The LS spectrum does not have mono-energetic features that could be used for energy calibration or estimation of the energy resolution. Therefore, in order to calculate the LS veto calibration factor, we compare the data to a simulated spectrum, over different

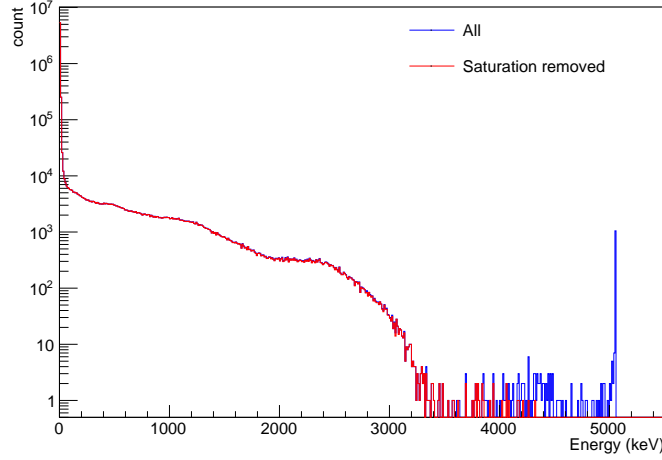


Figure 3: Liquid scintillator veto spectrum after calibration, with the added charge of the 18 PMTs (blue). Removing the PMTs’ saturated events (red) does not affect spectral shape below  $\sim 3.2$  MeV.

resolution functions. In the simulated spectrum we consider the energy deposited in the LS by all the detector’s materials. We also compare crystal-LS coincidence spectra, selecting a specific group of events that could be tagged by both crystal and LS. For example, we select  $^{40}\text{K}$  events which have 3.2 keV auger electrons deposited in the crystals and higher energy (up to 1460 keV) events in the LS. The shoulder around 1460 keV is then matched between the simulation and data, to determine an estimation of resolution and calibration. The comparison between data and simulation is shown in Fig 4.

## 5. Background Fit

Once the calibration and resolution are estimated, the LS background can be modeled with a full spectrum fit. The Geant4 [16, 17] simulated spectrum consists of components from crystals, PMTs, the LS itself and other external components. Each component is simulated separately. Since the LS is currently being used in the passive mode, a selection must be applied to identify only the events depositing energy in at least one crystal.

The fitting is done with a standard likelihood fit, taking into consideration various simulated spectra and statistical uncertainties in data. Only the energy region between 500-3000 keV is fitted, since the resolution was estimated uniquely for the higher energies.

The fit considers initial estimation of the background levels, which are given in [18]. The exception for that is the  $^{40}\text{K}$  in the LS. We compare that component with recent measurements. Only 100 hours of data are used in the fit, to avoid spectral changes due to gain drift. The fitted simulation spectra can be seen in Fig. 5, while the background levels are given in Table 1.

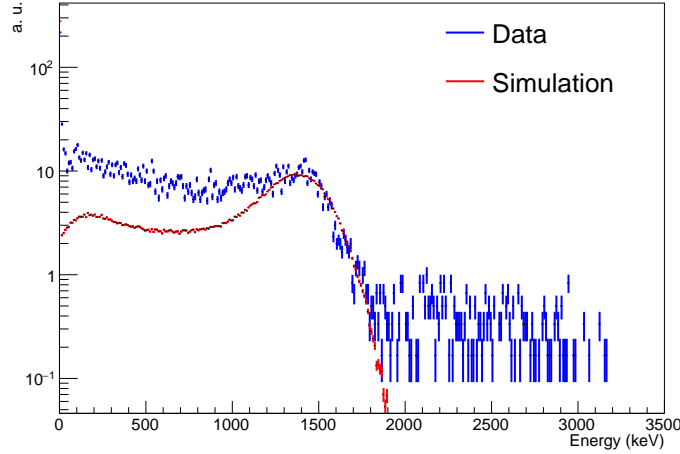


Figure 4: Liquid scintillator veto tagging spectra for crystal events with energies between 2-4 keV. The comparison between data (blue) and simulation (red) is shown at arbitrary rate scale. The data spectrum has higher rates at lower energies due to other background components that can act at those energies. At energies above  $\sim 1.9$  MeV, events cannot be attributed to  $^{40}\text{K}$  only, so they must correspond to decays of other components or wrong coincidence.

## 6. Analysis Threshold Estimation

The single and multiple hit event selection require an energy analysis threshold for the LS channel data. However, since the total charge of the LS is always recorded when there is a crystal trigger (there is always a total LS charge associated to a crystal event), one must determine which LS events are real coincidence and which are due to noise or fluctuations. One way to assess this is by analysing the total rate dependence over the LS total charge integral (or event energy), which is expected to drop as energy increases due to the higher amount of noise at lower energies. The LS analysis threshold is then estimated based on the energy at which LS noise events do not affect the total multiple hit rate of the crystals. This means that above that threshold all the LS events will be considered real coincidence events with the crystals' signals.

Data from LS is recorded when at least one crystal is triggered (passive trigger) or when both the LS and at least one muon detector are triggered (active trigger) [8]. LS charge is digitized every 16 ns (sample time). When the channel is locally triggered, the input signal is integrated over the following 192 ns. Local triggers may not, however, correspond to the recorded data rate, since coincidence conditions have to be respected (see conditions described in [8]). The  $\sim 200$  ns/event is the intrinsic dead time of the LS, meaning that no trigger happens within that integration time. The amount of noise in LS channels can, therefore, affect the total dead time of the detector in the active trigger configuration. The analysis threshold can be estimated by taking a conservative assumption that the LS dead time should not contribute to more than 0.5% of the LS rate at saturation point.

Considering the 200 ns/event integration time, the LS channels saturate fully at 5 MHz. Nonetheless, since the energy threshold desired is for crystal-LS coincidence events, that is

Table 1: Background fitting results.

Component	Background (mBq/kg)
Internal $^{40}\text{K}$	$7.04 \pm 10.9$
Internal $^{22}\text{Na}$	$0.63 \pm 11.8$
PMT $^{238}\text{U}$	$3.84 \pm 13.5$
PMT $^{232}\text{Th}$	$75.4 \pm 54.9$
PMT $^{40}\text{K}$	$32.5 \pm 19.1$
LS $^{40}\text{K}$	$5.9 \pm 54.0$
LS $^{238}\text{U}$	$0.09 \pm 0.08$
LS $^{232}\text{Th}$	$0.02 \pm 0.02$
External Steel $^{238}\text{U}$	$29.4 \pm 346.0$
External Steel $^{232}\text{Th}$	$49.1 \pm 173.2$

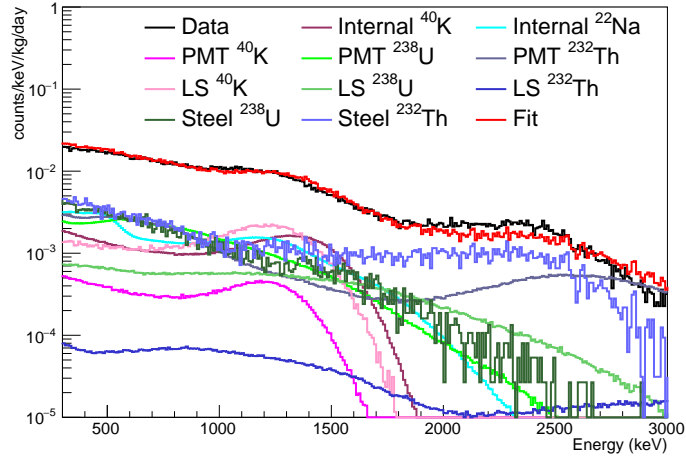


Figure 5: Fit of the first 100 hours of liquid scintillator data with Geant4 simulations for the main components in the detector. The main contributors for the two shoulders observed in the spectra are the  $^{40}\text{K}$  in the LS and the external  $^{208}\text{Tl}$ .

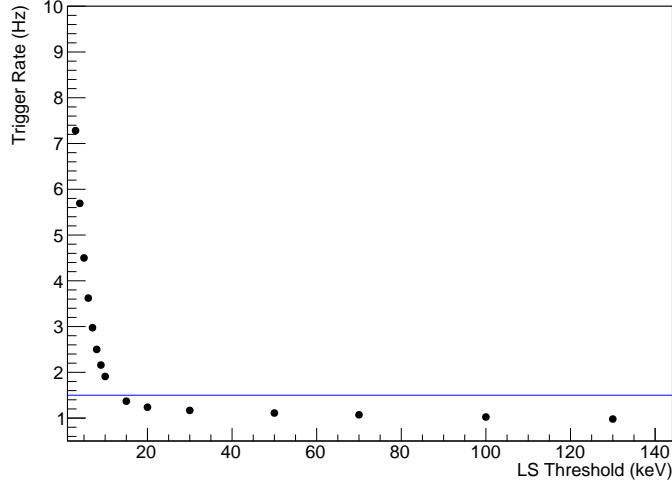


Figure 6: LS trigger rate as a function of LS threshold. The line is drawn at 1.5 Hz, which represents 0.5% deadtime of LS DAQ.

not the total rate that should be considered. The trigger rate of the crystals is approximately 15 Hz in average, which results in the LS coincidence events also having that rate. For each crystal trigger, a  $4 \mu\text{s}$  window is open in the LS channels to search for the maximum integrated charge for each of them, resulting in a total window of  $60 \mu\text{s}$  per second. This means that only the noise events in that time fraction are able to affect our coincidence energy threshold, bringing the 5 MHz down to 300 Hz, as  $5 \text{ MHz} \times 60 \mu\text{s}/\text{second} = 300 \text{ Hz}$ , the total rate at which we have 100% dead time. With the above assumption to keep the dead time at the maximum of 0.5%, it would correspond to setting an analysis threshold at the LS energy where the rate is below 1.5 Hz. Figure 6 shows how the LS total trigger rate changes as a function of the threshold. With a higher analysis threshold, the LS trigger rate decreases as less events pass that energy threshold. This demonstrates that by having a threshold of 20 keV, you can achieve  $<0.5\%$  dead time in the LS channels.

## 7. Background Tagging Efficiency

The tagging efficiency is defined as the fraction of events tagged (vetoed) by the LS among all the triggered events in the crystals. In order to estimate the tagging efficiency of the LS system in COSINE-100, we count the event rates of the NaI(Tl) detectors with and without the LS veto requirement, as shown in Fig. 7. The detectors realize a significant reduction in the background rate by requiring that no signal appear in the LS veto detector. The total tagging efficiency of six active crystals in the COSINE-100 system, which is calculated with the total number of LS-tagged events, is shown in Table. 2, for 6–20 and 100–1500 keV energy regions. Two crystals, Crystal-5 and Crystal-8, are not shown due to their lower light yields and hence the higher energy thresholds (4 keV and 8 keV) [4]. The total tagging efficiencies of the LS are between 10% and 16% in the low energy region and between 50%



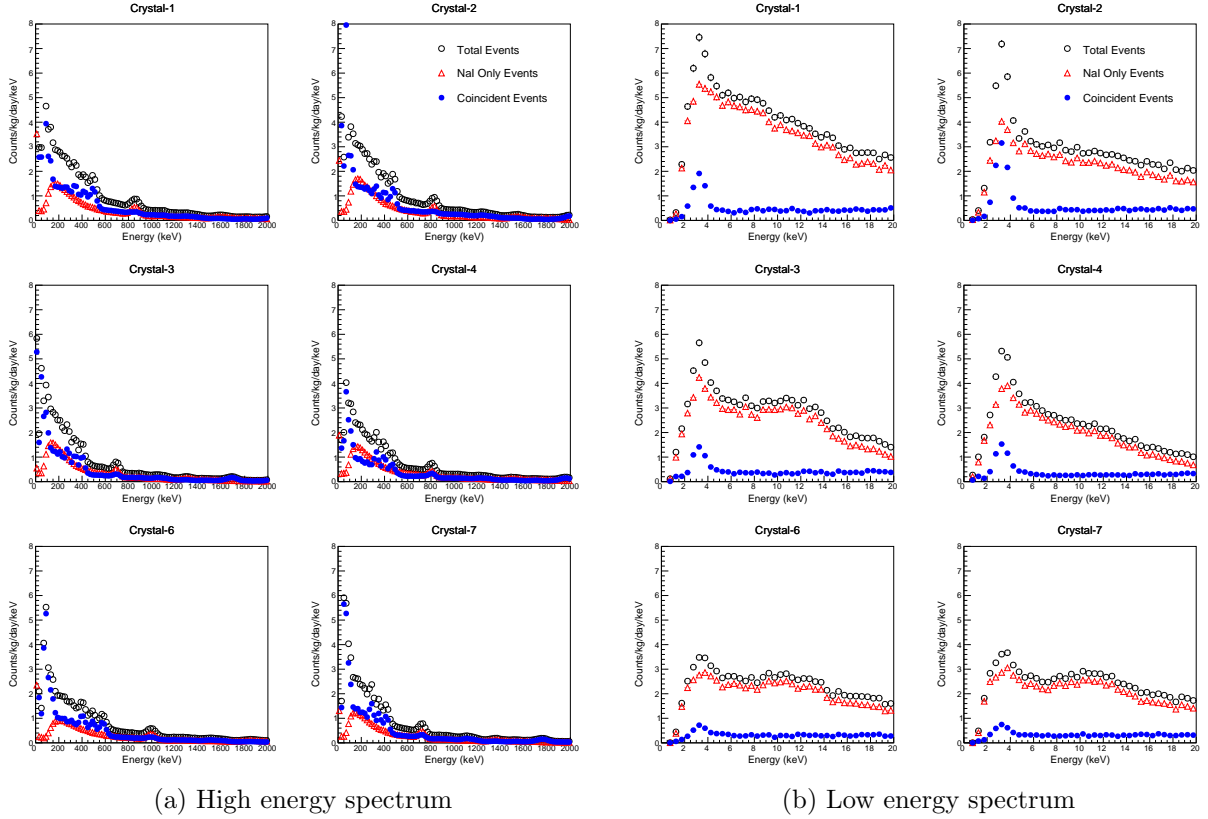


Figure 7: Background energy spectra of the six NaI(Tl) crystals in the COSINE-100 detector system, for high (a) and low energy (b). Vetoed events (blue filled circles) have hits on the LS veto detector with energies greater than 20 keV, whereas hits on NaI only (red triangles) have no such hits on the LS veto detector. The total hits (black open circles) represents all events (the sum of events in both categories). The other two crystals, Crystal-5 and Crystal-8, are not shown due to their lower light yields and hence the higher energy thresholds.

and 62% in the high energy region, for different crystals in the detector system. This can be clearly observed in Fig. 7 by comparing rates of the coincident events and the total events. The tagging efficiencies in the energy interval of 2–6 keV are higher than those in the 6–20 keV, which indicates that the efficiency of tagging  $^{40}\text{K}$  with LS is higher than that of the other components.

One of prominent backgrounds for dark matter searches with NaI(Tl) crystals is the internal  $^{40}\text{K}$  decay into  $^{40}\text{Ar}$  [19, 4, 20, 21, 22, 23]. This decay generates an X-ray at approximately 3.2 keV with a 1460 keV  $\gamma$ -ray. If the accompanying 1460 keV  $\gamma$ -ray escapes from the crystal, the event consists of a single 3.2 keV hit, which becomes a background in the region of interest for WIMP search. However, if we tag the escaping 1460 keV  $\gamma$ -ray with the LS veto detector, we can effectively reduce the low-energy contribution of the 3.2 keV X-ray in the NaI(Tl) crystal.

In order to properly obtain this  $^{40}\text{K}$  tagging efficiency of the LS system, we need to simulate various background sources with the Geant4 simulation package. The veto efficiency

Table 2: Total tagging efficiencies for six crystals in COSINE-100 detector system, calculated from the data.

Total tagging efficiency (%)	Crystal-1	Crystal-2	Crystal-3	Crystal-4	Crystal-6	Crystal-7
6–20 keV	10.88	16.52	13.98	14.39	13.06	13.15
100–1500 keV	57.53	54.69	50.92	49.79	61.92	57.68

for energies between 2–4 keV is estimated from the internal  $^{40}\text{K}$  simulation, which shows that the tagging efficiency of the  $^{40}\text{K}$  events is 65 – 75%. The un-tagged  $^{40}\text{K}$  events are due to 1460 keV  $\gamma$ -rays escaping completely the LS Veto, or escaping towards the crystals' PMTs (and scattering there), or even due to  $^{40}\text{K}$  decays into  $^{40}\text{Ca}$  instead of  $^{40}\text{Ar}$ . The  $^{40}\text{K}$  tagging efficiencies of Crystal-1 (75.1%) and Crystal-4 (75.9%) are found to be higher than the other crystals, since these two crystals are located at the edges of the array and hence the surrounding LS volume is larger, as shown in 1b. The efficiencies of Crystal-6 (66.5%) and Crystal-7 (65.8%), on the other hand, are the lowest as they are at the bottom layer and surrounded by neighboring crystals. The filled (blue) circles in Fig. 7b show the low-energy spectrum of the NaI(Tl) crystal that is tagged by the LS veto detector. The size of the 3.2 keV peak from  $^{40}\text{K}$  decay differs based on the crystal due to the difference in initial  $^{40}\text{K}$  contamination levels in each of them, where Crystal-2 has the highest level of  $^{40}\text{K}$  contamination, followed by Crystal-1/Crystal-3/Crystal-4 and Crystal-6/Crystal-7 [4].

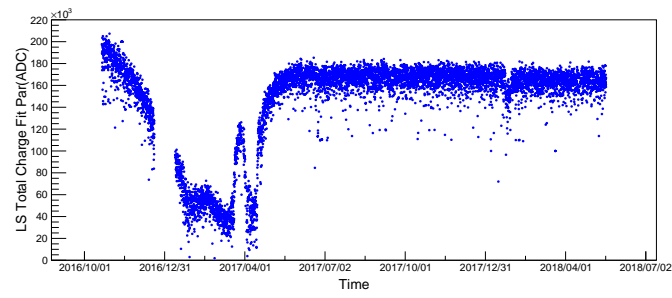
## 8. Gain fluctuation and correction

The LS gain can be monitored by tracking a Compton edge of  $^{40}\text{K}$  over time. To quantitatively evaluate the LS gain, we fit the Compton edge of  $^{40}\text{K}$  found in the LS spectrum with the following function,

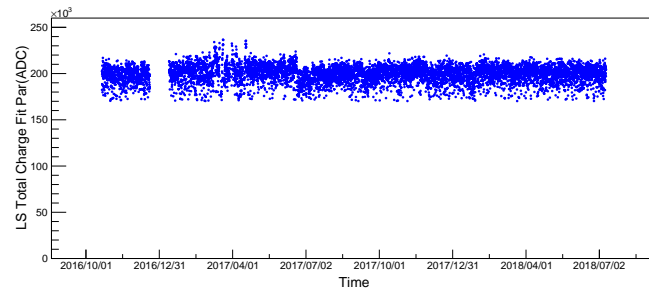
$$y = \frac{p_0}{e^{p_1(x-p_2)} + 1}, \quad (1)$$

and extract the  $p_2$  parameter which represents a location of the Compton edge. The plot of the parameter  $p_2$  as a function of time is shown in Fig. 8a, and it was observed that the gain slowly starts to decrease from the beginning of the physics run and it hits the minimum at around early April 2017 while the gain fluctuates in between. Then the gain increases back to 85% of the original gain at around late June 2017, and has been slowly dropping since.

We have not found the cause of this behavior, as there are only limited information of LS system that can be gained from the current detector DAQ configuration where we only save charge sum of a triggered event. However, it is important to correct the LS gain as it will impact the signal event selection of COSINE-100. We took the  $p_2$  parameter from the LS spectrum of the first dataset of the physics run as a reference, then corrected the rest of the datasets by correcting the same fit parameter. The fit parameters from the corrected LS spectrum as a function of time can be found in Fig. 8b where the trend is improved after the correction.



(a) LS gain vs. Time before the correction



(b) LS gain vs. Time after the correction

Figure 8: LS gain fluctuation as a function of time before (a) and after the correction (b). The gain of LS is represented by a location of Compton edge originated from  $^{40}\text{K}$ .

## 9. Conclusion

The main purpose of the LS veto system of the COSINE-100 experiment is to reduce the background level both from the external and internal sources. The liquid scintillator is carefully produced to have high light yield with low radioactive background. The data with a total exposure of 59.5 live days were used for this analysis. A Geant4 simulation shows a good agreement with the data measured from the LS system, and this simulation result is then used to cross-check the calibration of the LS. The analysis threshold is estimated to minimize noise events contamination in event selection. The tagging efficiency of the 3.2 keV X-rays from internal  $^{40}\text{K}$  is estimated to be about 65 to 75% from the Geant4 simulation.

## acknowledgements

We thank the Korea Hydro and Nuclear Power (KHNP) company for providing the underground laboratory space at Yangyang. This research was funded by the Institute for Basic Science (IBS) under project code IBS-R016-A1 and NRF-2016R1A2B3008343, Republic of Korea; an Alfred P. Slone Foundation Fellowship; NSF Grant Nos. PHY-1151795, PHY-1457995, DGE-1122492, and DGE-1256259; the Wisconsin Alumni Research Foundation; UIUC Campus Research Board; Yale University; and DOE/NNSA Grand No. DE-FC52-08NA28752, United States; STFC Grant ST/N000277/1 and ST/K001337/1, United Kingdom; and grant No.2017/02952-0, São Paulo Research Foundation (FAPESP), CAPES Finance Code 001, Brazil.

We thank the Korea Hydro and Nuclear Power (KHNP) Company for providing underground laboratory space at Yangyang. This work is supported by: the Institute for Basic Science (IBS) under project code IBS-R016-A1 and NRF-2016R1A2B3008343, NRF-2018R1D1A1B07048941, Republic of Korea; NSF Grants No. PHY-1913742, DGE-1122492, WIPAC, the Wisconsin Alumni Research Foundation, United States; STFC Grant ST/N000277/1 and ST/K001337/1, United Kingdom; Grant No. 2017/02952-0 FAPESP, CAPES Finance Code 001, CNPq 131152/2020-3, Brazil.

## References

- [1] P.A.R. Ade et al. Planck 2013 results. xvi. cosmological parameters. *Astron. Astrophys.*, 571:A17, 2014.
- [2] Gianfranco Bertone, Dan Hooper, and Joseph Silk. Particle dark matter: Evidence, candidates and constraints. *Phys. Rep.*, 405:279–390, 2005.
- [3] Gary Steigman and Michael S. Turner. Cosmological constraints on the properties of weakly interacting massive particles. *Nucl. Phys.*, B253:375, 1985.
- [4] G. Adhikari et al. Initial performance of the COSINE-100 experiment. *Eur. Phys. J. C*, 78:107, 2018.
- [5] R. Bernabei et al. Dark matter particles in the Galactic halo: Results and implications from DAMA/NaI. *Int. J. Mod. Phys. D*, 13:2127–2160, 2004.
- [6] R. Bernabei et al. Final model independent result of DAMA/LIBRA-phase1. *Eur. Phys. J. C*, 73:2648, 2013.
- [7] R. Bernabei et al. First model independent results from DAMA/LIBRA-phase2. *Universe*, 11:116, 2018.
- [8] G. Adhikari et al. The COSINE-100 Data Acquisition System. *JINST*, 13:P09006, 2018.

- [9] P.K. Lightfoot et al. Development of a gadolinium-loaded liquid scintillator for solar neutrino detection and neutron measurements. *Nucl. Instrum. Methods Phys. Res., Sect. A* 522:439, 2004.
- [10] J.S. Park et al. Performance of a prototype active veto system using liquid scintillator for a dark matter experiment. *Nucl. Instrum. Methods Phys. Res., Sect. A* 851:103–107, 2017.
- [11] J.S. Park et al. Production and optical properties of Gd-loaded liquid scintillator for the RENO neutrino detector. *Nucl. Instrum. Methods Phys. Res., Sect. A* 707:45–53, 2013.
- [12] M. Yeh. Gadolinium-loaded liquid scintillator for high-precision measurements of antineutrino oscillations and the mixing angle,  $\theta_{13}$ . *Nucl. Instrum. Methods Phys. Res., Sect. A* 578:329, 2007.
- [13] S.C. Kim et al. New Limits on Interactions between Weakly Interacting Massive Particles and Nucleons Obtained with CsI(Tl) Crystal Detectors. *Phys. Rev. Lett.*, 108:181301, 2012.
- [14] G. Adhikari et al. Study of fast neutron detector for COSINE-100 experiment. *JINST*, 13:T06005, 2018.
- [15] K.W. Kim et al. Tests on NaI(Tl) crystals for WIMP search at the Yangyang Underground Laboratory. *Astropart. Phys.*, 62:249, 2015.
- [16] S. Agostinelli et al. GEANT4—a simulation toolkit. *Nucl. Instrum. Methods Phys. Res., Sect. A* 506:250, 2003.
- [17] J. Allison and other. Geant4 developments and applications. *IEEE Trans. Nucl. Sci.*, 53:270, 2006.
- [18] P. Adhikari et al. Background model for the NaI(Tl) crystals in COSINE-100. *Eur. Phys. J. C*, 78(6):490, 2018.
- [19] E. Barbosa de Souza et al. First search for a dark matter annual modulation signal with NaI(Tl) in the Southern Hemisphere by DM-Ice17. *Phys. Rev. D.*, 95:032006, 2017.
- [20] G. Adhikari et al. An experiment to search for dark-matter interactions using sodium iodide detectors. *Nature*, 564:83–86, 2018.
- [21] J. Amaré et al. Preliminary results of ANAIS-25. *Methods Phys. Res. Sect. A*, 742:187, 2014.
- [22] J. Amaré et al. Assessment of backgrounds of the ANAIS experiment for dark matter direct detection. *Eur. Phys. J. C*, 76:429, 2016.
- [23] F. Froberg et al. SABRE: WIMP modulation detection in the northern and southern hemisphere. *J. Phys. Conf. Ser.*, 718:042021, 2016.